

The Craniofacial Phenotype of the Crouzon Mouse: Analysis of a Model for Syndromic Craniosynostosis Using Three-Dimensional MicroCT

Chad A. Perlyn, M.D., Valerie B. DeLeon, Ph.D., Christian Babbs, D.Phil., Daniel Govier, Lance Burell, Tron Darvann, Ph.D., Sven Kreiborg, D.D.S., Ph.D., Dr.Odont., Gillian Morriss-Kay, Ph.D., D.Sc.

Objective: To characterize the craniofacial phenotype of a mouse model for Crouzon syndrome by a quantitative analysis of skull morphology in mutant and wild-type mice and to compare the findings with skull features observed in humans with Crouzon syndrome.

Methods: MicroCT scans and skeletal preparations were obtained on previously described *Fgfr2*^{C342Y/+} Crouzon mutant mice and wild-type mice at 6 weeks of age. Three-dimensional coordinate data from biologically relevant landmarks on the skulls were collected. Euclidean Distance Matrix Analysis was used to quantify and compare skull shapes using these landmark data.

Results: Obliteration of bilateral coronal sutures was observed in 80% of skulls, and complete synostosis of the sagittal suture was observed in 70%. In contrast, fewer than 40% of lambdoid sutures were found to be fully fused. In each of the 10 *Fgfr2*^{C342Y/+} mutant mice analyzed, the presphenoid-basisphenoid synchondrosis was fused. Skull height and width were increased in mutant mice, whereas skull length was decreased. Interorbital distance was also increased in *Fgfr2*^{C342Y/+} mice as compared with wild-type littermates. Upper-jaw length was shorter in the *Fgfr2*^{C342Y/+} mutant skulls, as was mandibular length.

Conclusion: Skulls of *Fgfr2*^{C342Y/+} mice differ from normal littermates in a comparable manner with differences between the skulls of humans with Crouzon syndrome and those of unaffected individuals. These findings were consistent across several regions of anatomic interest. Further investigation into the molecular mechanisms underlying the anomalies seen in the Crouzon mouse model is currently under way.

KEY WORDS: *Crouzon syndrome, FGFR2, fibroblast growth factor receptor, mouse model, three-dimensional imaging*

Crouzon syndrome was first described nearly 100 years ago in a mother and her 3-year-old son, both presenting malfor-

Dr. Perlyn is Plastic Surgery Resident, Division of Plastic Surgery, Washington University School of Medicine, St. Louis, Missouri. Dr. DeLeon is Assistant Professor, Center for Functional Anatomy and Evolution, Johns Hopkins University, Baltimore, Maryland. Dr. Babbs is Postdoctoral Fellow, Weatherall Institute of Molecular Medicine, University of Oxford, Oxford, United Kingdom. Mr. Govier is Research Assistant, Division of Plastic Surgery, Washington University School of Medicine, St. Louis, Missouri. Mr. Burell is Coordinator, Micro CT Imaging Facility, University of Utah, Salt Lake City, Utah. Dr. Darvann is Research Engineer, School of Dentistry, University of Copenhagen, Copenhagen, Denmark. Dr. Kreiborg is Professor, School of Dentistry, University of Copenhagen, Copenhagen, Denmark. Dr. Morriss-Kay is Professor, Department of Physiology, Anatomy, and Genetics, University of Oxford, Oxford, United Kingdom.

Drs. Perlyn and DeLeon contributed equally to this work and share first authorship. Funding for this research was provided by an American College of Surgeons Research Fellowship and a Plastic Surgery Educational Foundation Research Grant.

Submitted December 2005; Accepted March 2006.

Address correspondence to: Dr. Chad A. Perlyn, Division of Plastic Surgery, c/o Department of Molecular Biology, Washington University School of Medicine, Campus Box 8103, 660 South Euclid Avenue, St. Louis, MO 63110. E-mail cperlyn@molcool.wustl.edu.

mations of the skull and the facial skeleton combined with exophthalmos and divergent strabismus (Crouzon, 1912). Crouzon (1912) suggested naming the condition “dysostose cranio-faciale héréditaire.” The syndrome was, however, not reported under the name of craniofacial dysostosis or Crouzon syndrome in the English language literature until 1939 (Krause and Buchanan, 1939). Later studies have shown varying degrees of premature fusion of sutures of the calvaria, cranial base, orbital region, and maxillary complex and even fusion of the synchondroses of the cranial base (Kreiborg, 1981a; Kreiborg and Björk, 1982; Kreiborg et al., 1993). The syndrome is characterized by progressive synostosis of sutures and synchondroses together with progressive calcification in the region of the cervical column and stylohyoid ligament (Kreiborg, 1981a; Kreiborg et al., 1993; Kreiborg, 2000). The facial phenotype is highly variable but is characterized by varying degrees of exophthalmos, hypertelorism, divergent strabismus, maxillary hypoplasia, narrow and high arched palate, mandibular overjet, and severe dental crowding, especially in the upper arch. The facial dysmorphology has been shown to progress during the growth period (Kreiborg, 1981a). Functional problems may include progressive hydrocephalus, increased

intracranial pressure, visual loss, breathing difficulties, and chewing problems (Cohen, 2000). Sequelae from obstructive sleep apnea may include failure to thrive or growth deficiency, hypertension, cardiorespiratory failure, and neurologic damage (Don and Sigger, 1971; Qvist et al., 2004).

Activating mutations in the gene encoding fibroblast growth factor receptor type 2 (*FGFR2*) have been identified in patients with Crouzon syndrome (Reardon et al., 1994; for review see Wilkie, 1997; Cohen, 2003). Some such patients additionally have a skin condition called acanthosis nigricans; these cases are due to a mutation in a different but closely related gene, *FGFR3* (Wilkes et al., 1996). The most common mutation in patients with Crouzon syndrome results in a change from cysteine to tyrosine at amino acid position 342 (Cys342Tyr; C342Y) (Wilkie, 1997). Recently a mouse model was created to study this mutation (Eswarakumar et al., 2004). Heterozygous *Fgfr2*^{C342Y/+} mice are characterized by a rounded calvaria, premature fusion of the cranial sutures, proptotic eyes, shortened midface, and high arched palate or cleft palate (<5%). Premature fusion of the cranial sutures is invariant at the coronal suture, with partial fusion of the lambdoid and sagittal sutures. *Fgfr2*^{C342Y/C342Y} mice show more severe craniofacial anomalies at birth, including cleft palate in more than 95% of pups. They die during the first postnatal day, likely because of respiratory distress associated with anomalies of the tracheobronchial tree.

The specific aims of this study were (1) to follow up the initial characterization of the *Fgfr2*^{C342Y/+} mouse (Eswarakumar et al., 2004) with an in-depth, quantitative analysis of the differences in skull morphology between mutant and wild-type mice and (2) to compare the findings with the skull features observed in humans with Crouzon syndrome (all of whom are heterozygous for the mutation). This was carried out by means of three-dimensional (3D) analysis based on MicroCT scan data.

The use of MicroCT for analysis of mutant mouse models is becoming increasingly popular (Ford-Hutchinson et al., 2003), with both simple screening techniques (e.g., linear measurements) and more complex forms of analysis (e.g., geometric morphometrics) being utilized. The patency status of mouse cranial sutures has also been evaluated by this technique (Recinos et al., 2004). Quantifying the growth disturbances seen in the mouse model is of interest for several reasons. It is well established that although many mouse models successfully genocopy a human condition, the expressed phenotype does not always parallel that seen in affected humans with the same mutation. One goal of this study was therefore to validate the mouse model as an appropriate tool for understanding Crouzon syndrome by demonstrating direct parallels between the dysmorphology of mouse and human craniofacial regions in affected individuals. Secondly, accurate, precise numerical quantification of the maxillocraniofacial anomalies, using 3D coordinates of biologic landmarks on the skull, is a necessary prerequisite to future work on therapeutic strategies, such as the development of pharmacologic interventions. The outcome of all such further studies will be based on a statistical



FIGURE 1 Wild-type mouse (right) and mouse with *Fgfr2*^{C342Y/+} mutation (left). Note the rounded calvaria and midface shortening associated with premature suture fusion.

comparison of the untreated and treated animals, with the intention that the treated animals become more similar to their wild-type littermates than untreated animals. Thus, establishing the “normative” values of the mutant mouse phenotype is a key component of all further work. For this purpose we have used two methods: (1) a rapid and efficient series of caliper-based skull measurements and (2) a more detailed analysis of size and shape by using an established morphometric method, Euclidean Distance Matrix Analysis (EDMA). The results provide insight into the nature of the specific craniofacial anomalies associated with Crouzon syndrome and further elucidate the relationship among distinct yet integrated parts of the developing skull.

METHODS AND MATERIALS

Fgfr2^{C342Y/+} mutant mice (Fig. 1) were a gift of the late Professor Peter Lonai (Weizmann Institute, Israel) and were constructed as described by Eswarakumar et al. (2004). All procedures were carried out in accordance with the United Kingdom Animals (Scientific Procedures) Act, guidelines of the Home Office, and regulations of the University of Oxford. Mutant mice of breeding age were determined by phenotype. Female mice that were heterozygotes for the *Fgfr2*^{C342Y} mutation were bred with males heterozygous for the same mutation. The genotype of each mouse was confirmed by performing polymerase chain reaction (PCR) analysis on DNA prepared from skin biopsies after sacrifice. To prepare DNA, tissue samples were digested at 55°C for 16 hours in 700 μ L of lysis buffer (50 mM Tris-HCl pH 8.0, 100 mM EDTA, 100 mM NaCl, 1% sodium dodecyl sulfate [SDS], 100 μ g/mL proteinase K). DNA was extracted once with phenol chloroform and extracted once with chloroform alone. DNA was precipitated with isopropanol and rinsed in 70% ethanol. DNA was resuspended in TE buffer (10 mM tris, 1 mM EDTA, pH 8.0) and amplified by PCR. Wild-type versus mutant genotype was determined by using primers specific to the region of interest (5'-GAGTAC CATGCTGACTGCATGC-3', P2 5'-GGAGAGGCATCTCTG TTTCAAGACC-3'). The wild-type allele was detected as a

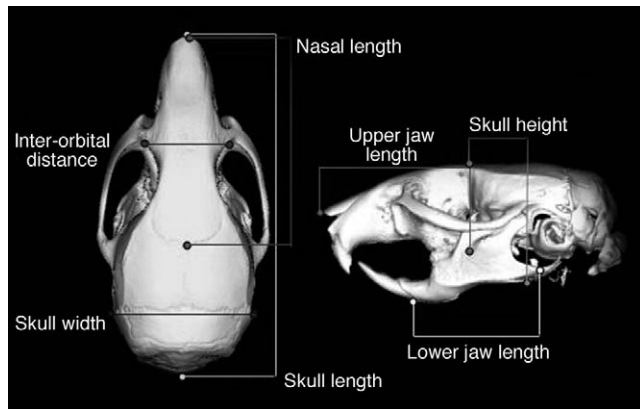


FIGURE 2 Linear-based measurements for analysis of the normal mouse skull. Adapted from Richtsmeier et al. (2000) and Craniofacial Resource, The Jackson Laboratory (www.jax.org/cranio/index.html).

224-bp amplification product and the mutant allele as a 290-bp product. Heterozygotes showed both the wild-type and mutant products.

Whole-mount skeletal preparations were prepared by first fixing each specimen in 95% ethanol for 1 to 3 days. Specimens were 6 weeks of age, which is the time mice reach sexual maturation, and were sacrificed by CO₂ asphyxiation. Skin and fur were dissected from the skulls, which were then immersed in alcian-blue stain (75% ethanol, 20% acetic acid, 3 mg/mL alcian blue) for 10 to 14 days at 37°C to stain cartilage. Differentiation was then carried out in 95% ethanol. Specimens were immersed into 1% potassium hydroxide (KOH) in dH₂O for 1 day and washed overnight in running tap water. Aqueous alizarin red stain (0.1%) was then used for 4 hours to stain bone. Excess stain was washed out with running tap water, and the samples were immersed in a solution of 1% KOH, 20% glycerol for clearing. After clearing they were dehydrated in ethanol and stored in a mix of 50% glycerol and 50% ethanol.

For 3D computed tomography (CT) scanning, 10 wild-type and 10 *Fgfr2*^{C342Y/+} specimens at 6 weeks of age (42 days) were sacrificed by CO₂ asphyxiation and were fixed in 95% ethanol. They were then sealed in conical tubes and shipped to the MicroCT imaging facility at the University of Utah. Images were obtained at 32 μm resolution with a General Electric Medical Systems EVS-RS9 MicroCT scanner (GEHealthcare, Waukesha, WI). Image data were then sent to the Craniofacial Imaging Laboratory (Perlyn et al., 2001) at the St. Louis Children's Hospital and the Developmental Genetics Laboratory at Johns Hopkins University and processed by using contemporary medical imaging software for qualitative and quantitative analyses of the craniofacial skeleton.

The relative degree of suture fusion was classified in all 10 heterozygotes. The right and left coronal, midline sagittal, and right and left lambdoid sutures were each analyzed individually to assess suture patency. Suture patency was classified as either (1) fully patent, (2) partially fused, or (3) fully obliterated. We used ANALYZE AVW software (Mayo Foundation for Medical Education and Research, Rochester, MN) to create 3D surface reconstructions from the CT data. Determination

TABLE 1 Cranial Landmarks for Which 3D Coordinate Data Were Collected

<i>Midline</i>	
nal	nasale
nas	nasion
pns	posterior nasal spine
pbm	presphenoid-basisphenoid external junction at midline
bom	basisphenoid-occipital external junction at midline
bas	basion
brg	bregma
lam	lambda (parietal/interparietal)
int	intersection of interparietal and occipital at midline
opi	opisthion
con	most anterior point on posterior edge between right and left optic canals
<i>Bilateral</i>	
pmm	most inferior point on premaxilla-maxilla suture
ppf	posterior palatine fissure
mxt	intersection of maxilla and sphenoid on inferior alveolar ridge
ptg	posteroinferior pterygoid bone (hamulus)
pss	posterior edge of alisphenoid-squamosal suture, anterior to bulla
alv	center of alveolar ridge over maxillary incisor
ast	asterion
not	anterior notch on frontal process lateral to infraorbital fissure
mfl	intersection of frontal process of maxilla with frontal and lacrimal bones
fsc	frontal-squamosal interjection at temporal crest
mjs	intersection of zygomatic process of maxilla with jugal, superior surface
jss	superiormost intersection of jugal with zygomatic process of squamosal

of suture patency was made by viewing the 3D reconstructions, as well as two-dimensional (2D) individual slices in orthogonal views throughout the length of the entire suture in question. This allowed for review of the sutures in a coronal, transverse, and sagittal plane to avoid a misinterpretation of suture patency that could result from volume averaging during the 3D reconstruction. Assessment made by analysis of the CT scan data was verified by evaluation under a dissecting microscope of skeletal preparations made from two specimens to confirm accuracy of the technique. An accuracy of 100% was determined by the CT method when compared with microscopic evaluation of the actual skull.

To obtain linear measurements, we used the 3D surface reconstructions created from the CT data in ANALYZE software. From these surfaces, a series of seven measurements were taken as described by Richtsmeier et al. (2000) and currently in use as the standard protocol for caliper measurements at the Craniofacial Mutant Resource Center of the Jackson Laboratory. These measurements include skull length, skull width, skull height, interorbital distance, nasal length, upper-jaw length, and lower-jaw length (Fig. 2). Although direct measurement is recommended for making linear measurements on the cleared skull as compared with 2D photographs (Hartsfield and Holmes, 1998), the accuracy of 3D computerized reconstructions in mice has been well documented (Lozanoff, 1992; Abe et al., 2000).

For a more detailed quantification of form, we collected 3D coordinate data from 35 biologically relevant landmarks on the skulls of the *Fgfr2*^{C342Y/+} mutant and wild-type samples (Table 1). Surface reconstructions were created from the MicroCT data described above, and coordinate data were collected by

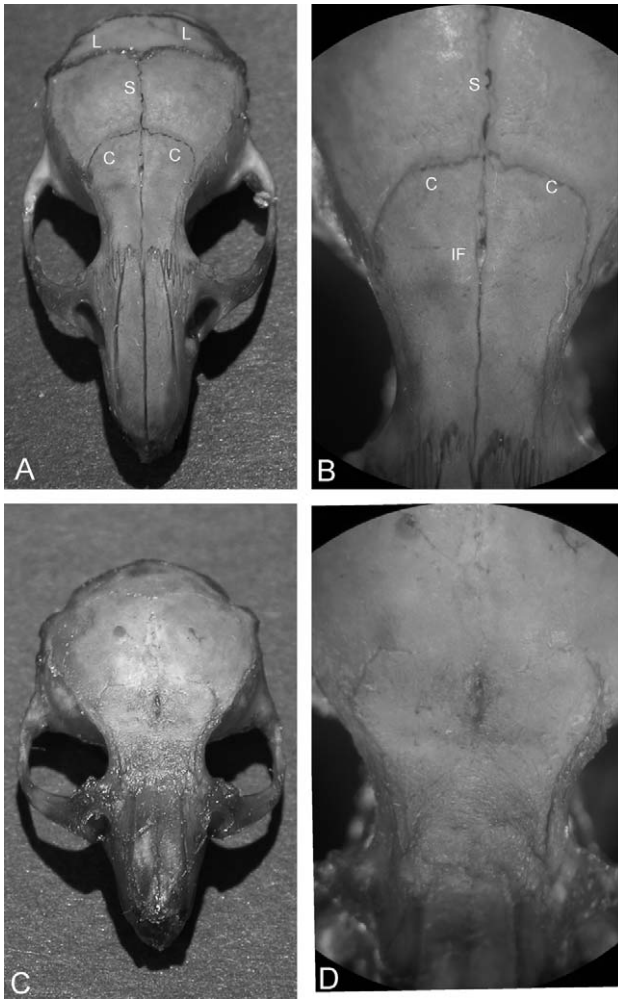


FIGURE 3 Skeletal preparation of 6-week-old wild-type (A, B) and *Fgfr2^{C342Y/+}* mutant mouse skulls (C, D). Note the nearly complete synostosis of all cranial sutures. C = coronal sutures; S = sagittal suture; L = lambdoid sutures; IF = interfrontal suture. There is a small patent part of the posterior frontal suture seen in the heterozygote specimen (C, D).

using the landmarking tool of eTDIPS software (available as freeware from the National Institutes of Health at <http://www.cc.nih.gov/cip/software/etdips/>). EDMA was used to quantify and compare the shape of the mutant skulls relative to the wild-type littermates by using these landmark data. EDMA is a geometric morphometric approach enabling the quantification and comparison of shape in three dimensions (Lele and Richtsmeier, 2001; <http://oshima.anthro.psu.edu/>) and has been applied in previous studies of craniofacial dysmorphology in humans (Richtsmeier et al., 1998; DeLeon et al., 2001) and mice (Richtsmeier et al., 2000). The form of each specimen in the sample was represented by a matrix of all possible interlandmark linear distances in the skull. Initially, differences in overall form were assessed using principal coordinates analyses (PCOORD), a data reduction application of EDMA that maps individuals in multidimensional space that is similar to a principal components analysis (Gower, 1966).

To investigate localized differences in shape, mean form matrices for each sample were calculated, and the mean forms

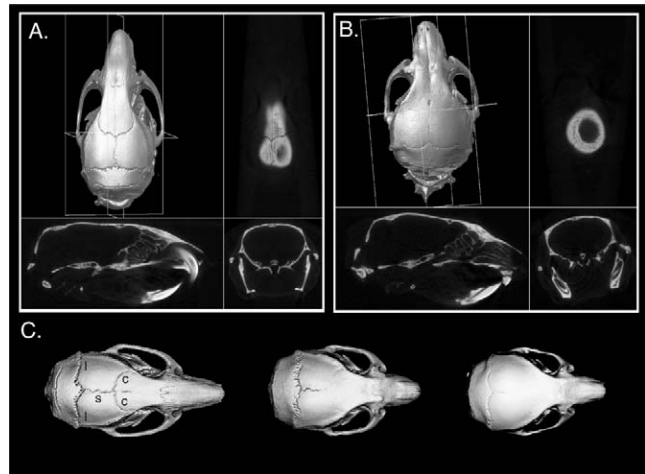


FIGURE 4 Patterns of suture fusion in 6-week-old mice. A: Calvaria of wild-type mouse shown as 3D surface reconstruction and in three-plane orthogonal views. B: Similar views of *Fgfr2^{C342Y/+}* mutant mouse. C: Skull on left is a wild-type skull, followed by two mutant skulls. Note the variability in the degree of fusion of the sagittal and lambdoid sutures in these two specimens. All analysis of suture patency from 3D reconstructed images was reviewed in the 2D slice data for confirmation.

were compared as ratios of matrix elements (Lele and Richtsmeier, 1991). Statistical significance of form differences was determined for each interlandmark linear distance by using confidence intervals, which were calculated by a nonparametric bootstrap method (Lele and Richtsmeier, 1995). For all EDMA results reported, the threshold for statistical significance was set at $\alpha = 0.01$.

RESULTS

Analysis of the alizarin red-stained skulls and the 2D and 3D CT scan data showed multiple suture fusion in all the *Fgfr2^{C342Y/+}* mice (Figs. 3 and 4). Complete obliteration of bilateral coronal sutures was observed in 80% of skulls, and complete synostosis of the sagittal suture was observed in 70%; in contrast, fewer than 40% of lambdoid sutures were found to be fully fused (Figs. 4 and 5). In each of the 10

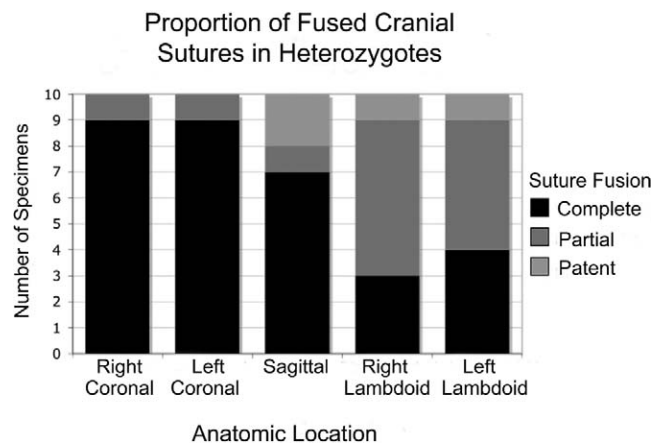


FIGURE 5 Analysis of suture fusion in *Fgfr2^{C342Y/+}* mutant mice.

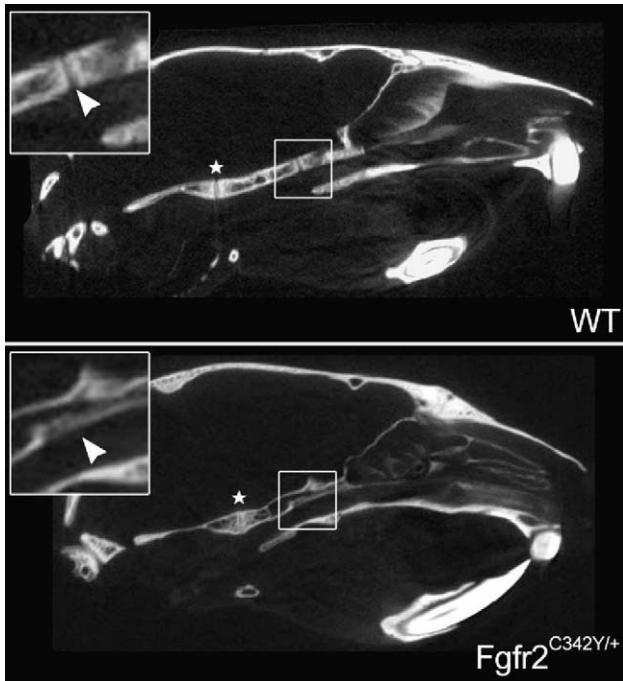


FIGURE 6 Sagittal sections from CT data of wild-type (top panel) and *Fgfr2*^{C342Y/+} (bottom panel) mice. The position of the presphenoid-basisphenoid sychondrosis is indicated by the smaller boxes and with white arrows in the inset magnified (3×) images. Note the complete obliteration of this suture in the *Fgfr2*^{C342Y/+} mouse. The basisphenoid-basioccipital sychondrosis is indicated with a white star in both panels for comparative purposes.

Fgfr2^{C342Y/+} mutant mice analyzed, the presphenoid-basisphenoid sychondrosis was fused, and in most it was completely obliterated (Fig. 6).

A consistent pattern of cranial dysmorphology in the *Fgfr2*^{C342Y/+} mice was observed (Fig. 7); linear measurements showed that skull height and width were increased in the mutant mice, whereas skull length was decreased, relative to values in wild-type skulls. Interorbital distance, a measurement to assess hypertelorism, was also slightly increased in *Fgfr2*^{C342Y/+} mice as compared with wild-type littermates. In addition, excessive ocular proptosis was noted in a majority of affected mice, with one individual developing a corneal opacity. Nasal, lower-jaw, and upper-jaw length were all found to be significantly reduced in the mutants as compared with wild-type mice, and a shortened tooth row was present in all affected individuals. The occlusal pattern of the molar teeth was similar to an Angle Class III appearance, with the mandibular dentition positioned mesially in relation to the maxillary dentition (Fig. 8). This necessitated clipping of the teeth in several mice because of the lack of normal abrasion.

Multivariate PCOORD indicated that the overall form of the *Fgfr2*^{C342Y/+} mutant skulls differed from that of the wild-type skulls (Fig. 9). Landmark coordinate data for all 20 specimens (10 *Fgfr2*^{C342Y/+} and 10 wild-type mice) were pooled into a single sample. According to these shape data, individuals were projected into multidimensional space by using the PCOORD application of EDMA, such that similarly shaped individuals

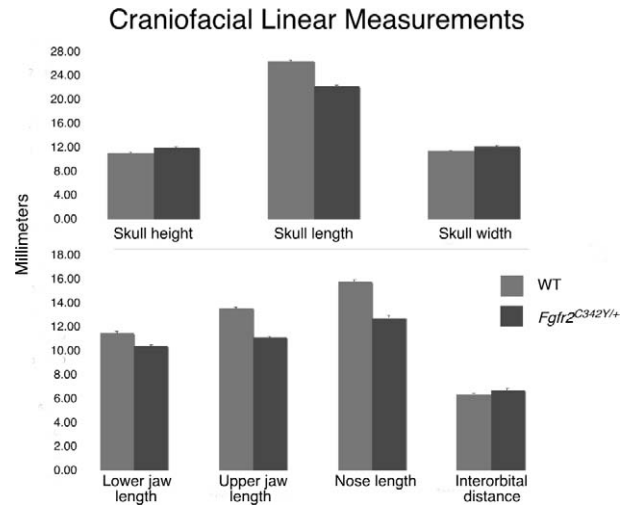


FIGURE 7 Results of linear measurements as indicated in Figure 3.

cluster more closely together. For purposes of visualizing these results, Figure 9 illustrates the distribution of all specimens along only the first two dimensions (axes). Almost all the shape variation among these individuals is represented by position on these two axes (axis 1 represents 81.6% of the total variation). The *Fgfr2*^{C342Y/+} mice cluster separately from the wild-type mice, indicating that overall shape of the *Fgfr2*^{C342Y/+} mutant skulls differs from that of the wild-type skulls.

EDMA analyses allowed us to localize the differences in

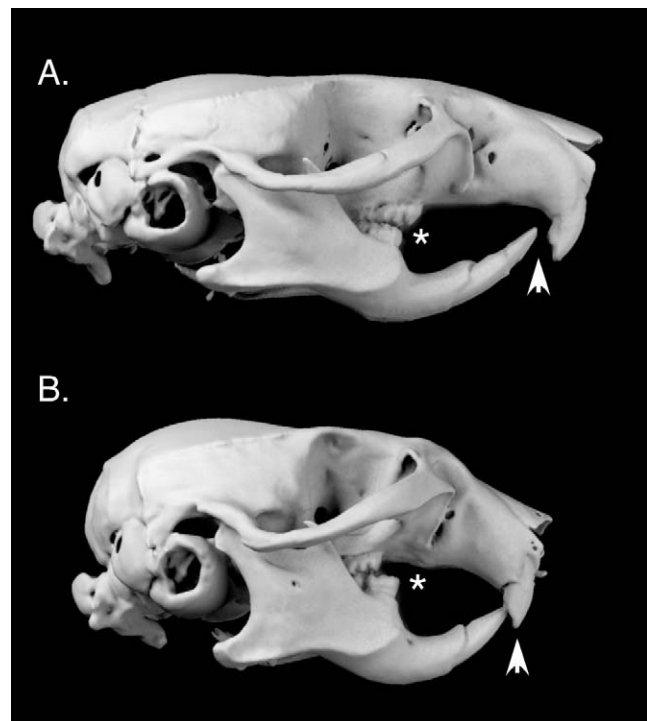


FIGURE 8 Pattern of dental occlusion in wild-type and *Fgfr2*^{C342Y/+} mutants. A: Wild-type mouse with appearance of Class I occlusion (*). B: Mutant mouse with Class III molar appearance (*). Arrows illustrate loss of incisor gap, indicating degree of maxillary retrusion.

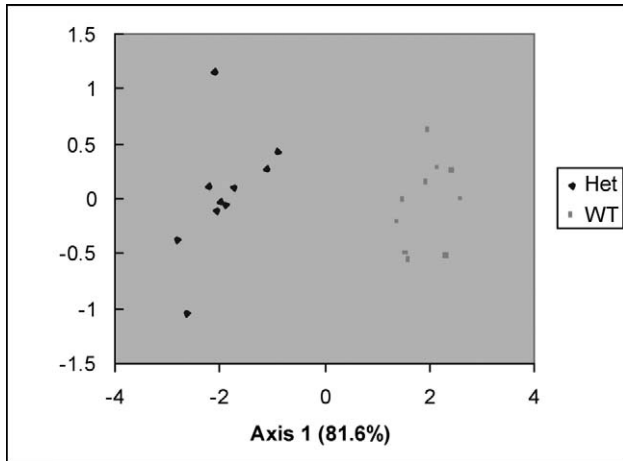


FIGURE 9 PCOORD analysis of all landmark data for all individuals in this study, $n = 20$ (10 *Fgfr2*^{C342Y/+} mice and 10 wild-type mice). Note the separation of the two samples along axis 1, which explains 81.6% of the variation among individuals. Data show that craniofacial phenotype of the mutant mice is distinctly different from that of the wild-type mice yet fairly consistent within the mutant population.

form associated with the *Fgfr2*^{C342Y/+} mutation. Results of the landmark-based form difference comparisons reiterated those obtained from traditional linear measurements (see Table 1 for abbreviations, with “R” for right and “L” for left). All results described here were statistically significant based on confidence intervals ($\alpha = 0.01$). Neurocranial width was significantly increased in mice with the *Fgfr2*^{C342Y/+} mutation (the distance Rfsc-Lfsc was 116% and Rast-Last was 108% that of normal). Neurocranial height was also significantly increased in the mutant mice (up to 115% that of wild-type mice, Fig. 10). In contrast, skull length was significantly decreased, resulting in a brachycephalic cranial morphology (Fig. 10). Upper-jaw length was found to be notably and significantly shorter in the *Fgfr2*^{C342Y/+} mutant skulls (Fig. 10). For example, the mean distance from the incisor alveoli to the posterior nasal spine (Lalv-pns, Ralv-pns) in the mutant skulls was less than 82% of that distance in wild-type mice. Interestingly, within the maxillary region, the nasal bones (nas-nal) and posterior palate (e.g., Lppf-pns, Rppf-pns) were significantly shorter in the mutant skulls (70% to 80%), but neither the length (97%) nor width (100%) of the premaxilla was significantly different between the mutant and wild-type skulls.

The most extreme form differences between the *Fgfr2*^{C342Y/+} mutant skulls and wild-type skulls were localized to the region of the anterior cranial base (Fig. 10). The posterior palate appears to be shifted posteriorly, such that distances from landmarks on the cranial base to the posterior palate (e.g., bom-pns, pbm-Rppf, pbm-Lppf) are less than 65% of comparable lengths in the wild-type skull. The anteroposterior length of the sphenoid bone or bones (e.g., bom-pbm, pbm-con) is reduced to 69% to 77% that of normal. In contrast, the anteroposterior length of the basioccipital (bas-bom) is identical to that in wild-type mice (100%).

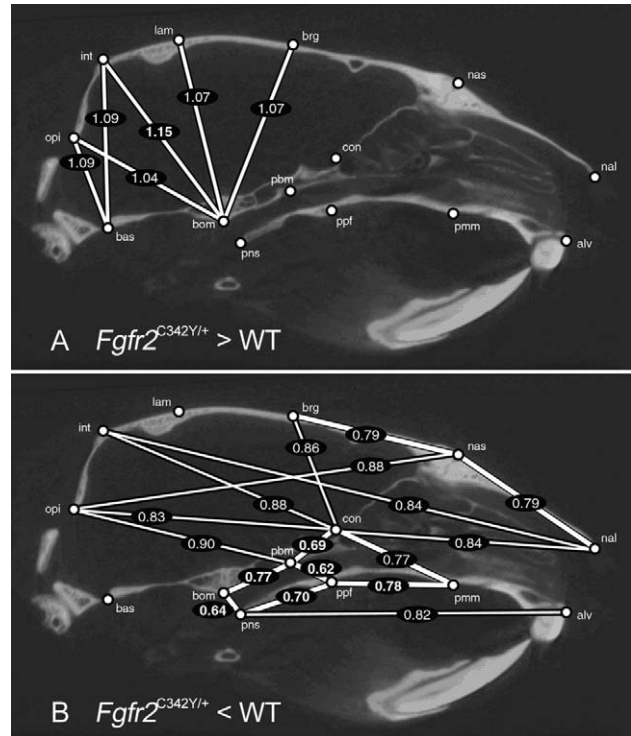


FIGURE 10 Results of EDMA form difference comparison. A subset of landmarks representative of the sagittal plane is shown on a sagittal CT section of an *Fgfr2*^{C342Y/+} mouse skull (anterior is to the right). Numbers represent the mean ratio of distance length in *Fgfr2*^{C342Y/+} mice to that in wild-type mice; landmark abbreviations are defined in Table 1. Panel A: A representative set of linear distances that are significantly greater in the *Fgfr2*^{C342Y/+} mice, relative to those of wild-type mice ($\alpha = 0.01$). Note the increased cranial height in the mutant mice. Panel B: A representative set of linear distances that are significantly less in the *Fgfr2*^{C342Y/+} mice, relative to wild-type mice ($\alpha = 0.01$). Note that the decreased cranial length in the mutant mice is most pronounced in the anterior cranial base and posterior palate. Two bilateral landmarks, pmm and ppf, are included here as informative regarding the midsagittal palate. Numbers reported for distances involving these bilateral landmarks are the least extreme (i.e., most conservative) of the right and left bilateral distances.

DISCUSSION

The development and initial characterization of the *Fgfr2*^{C342Y/+} mutant mouse was reported by Eswarakumar et al. (2004). Here, we set out to quantify the differences in skull morphology between *Fgfr2*^{C342Y/+} and wild-type mice and to assess their potential as a model for Crouzon syndrome in humans. Our results showed that the skulls of *Fgfr2*^{C342Y/+} mice differ from normal littermates in a parallel manner to that between the skulls of humans with Crouzon syndrome and those of unaffected individuals. These findings were consistent across several regions of anatomic interest, including the calvaria, endocranial base, orbital region, midface, and mandible, as discussed below.

Calvaria

The finding of multiple suture fusion and the pattern of craniosynostosis in the mutant mice are in agreement with the

findings observed in humans with Crouzon syndrome (Kreiborg, 1981a). The pattern of a wider, taller, and shorter skull in the mutant mice is consistent with the clinical appearance of brachycephaly, seen in humans with premature fusion of the coronal sutures bilaterally (e.g., in Crouzon syndrome) (Kreiborg, 1981a). In the original description of the mouse model (Eswarakumar et al., 2004), the age of evaluated affected specimens was 4 weeks. At this time point the coronal sutures were fused, there was partial fusion of the lambdoid sutures, and the sagittal suture was noted to be partially separable. In the current study, we have performed a detailed analysis of suture fusion at 6 weeks of age, a time that correlates with the onset of sexual maturity in mice. By this age, the sagittal suture was completely obliterated in 70% of specimens observed. This suggests that, as in the human condition, the synostosis associated with Crouzon syndrome progresses postnatally and that fusion of the coronal sutures is most precocious. Interestingly, there appear to be no functional deleterious effects of multiple suture fusion on murine brain development. Although neither cognitive testing nor neurohistologic studies were performed, affected heterozygotes have normal life spans, have appropriate social and behavioral interactions, and breed readily. The explanation may be related to the fact that mouse brain growth and maturation are completed much earlier than human brain development, possibly before the developmental insult created by the progressive fusion associated with the *Fgfr2*^{C342Y} mutation.

Endocranial Base

The sphenoid bone forms from multiple ossification centers; in normal humans these generally fuse into a single bone during the prenatal period. However, in normal adult mice, the sphenoid remains as distinct bones separated by synchondroses: the midline presphenoid and basisphenoid and two alisphenoid (greater wing) bones. The finding of abnormal fusion of synchondroses in the cranial base of the mutant mice is in agreement with the observation in humans with Crouzon syndrome showing premature fusion of the sphenoid-occipital and petro-occipital synchondroses (Kreiborg, 1981a; Kreiborg and Björk, 1982; Burdi et al., 1986; Kreiborg et al., 1993). Similar to findings in the cranial sutures, Eswarakumar et al. (2004) did not find complete obliteration of the skull base synchondroses at 4 weeks of age. However, by 6 weeks of age, fusion of the presphenoid–basisphenoid synchondroses was present, again suggesting the progressive nature of the deformities associated with this mutation. The findings in the endocranial base are of much interest because they provide a model for understanding, on a molecular and developmental level, the role of *FGFR2* in the formation and maturation of the cartilaginous synchondroses of the skull base.

Orbital Region

Findings of orbital hypertelorism, ocular proptosis, and corneal opacity in the mutant mice are also seen in humans with

Crouzon syndrome (Kreiborg 1981a; Okajima et al., 1999). A detailed morphometric anatomic analysis of the orbit itself was not performed, but observation suggests that the ocular proptosis results from shallow orbits.

Midface

Quantitative findings in the mutant mice of a smaller upper-jaw length with a shortened tooth row and Angle Class III malocclusion are similar to roentgencephalometric findings in humans with Crouzon syndrome (Kreiborg, 1981a; Carinci et al., 1994) and can likely be explained by premature fusion of maxillary sutures. In the mouse model, maxillary shortening was seen with the posterior palate being particularly affected (pmm-ppf <78% and ppf-pns <70% of normal) and shifted posteriorly relative to the cranial base (pns-bom 64% of normal). Interestingly, the length of the premaxilla did not appear to be affected (alv-pmm was 97% of normal). Roentgencephalometric studies in humans with Crouzon syndrome have revealed a reduction in volume and height of the rhinopharynx, with reduction of the size of the nasal cavities and nasal height (Kreiborg, 1981a; Carinci et al., 1994). These findings were also seen in the mice, with shortening of the nasal bones and of the nasal cavity.

Reduction in the dimensions of the nasal cavity and rhinopharynx has been associated with obligate mouth breathing in many humans with Crouzon syndrome (Kreiborg, 1981a), which again can lead to obstructive sleep apnea and other respiratory difficulties (Don and Sigger, 1971; Qvist et al., 2004). Many of the mice exhibited respiratory distress as well, as evidenced by frequent upper respiratory tract infections and chronic wheezing. However, it is our impression that this is primarily related not to the above anomalies but to fusion of the cartilaginous rings of the trachea and upper bronchi (Eswarakumar et al., 2004). This aspect of the mouse phenotype, which has also been documented in humans with Crouzon and Apert syndromes (Devine et al., 1984; Cohen and Kreiborg, 1992), is now the study of further investigation in our laboratory.

Mandible

Mandibular length was decreased in the mutant mice, reflecting the findings of Kreiborg (1981a), who reported reduced mandibular length in men and women with Crouzon syndrome when compared with normal controls. The difference was, however, significant only for women. Eswarakumar et al. (2004) suggested that the short mandible in the mutant mice does not reflect micrognathia or retrognathia but rather a generalized decrease in bone size seen throughout the affected animals. Kreiborg (1981a, 1981b) described normal mandibular growth in children with Crouzon syndrome and suggested that the mild mandibular shortening could be the result of mandibular adaptation to the short middle cranial fossa found in these patients.

In conclusion, the present study showed that the craniofacial

phenotype in the Crouzon mouse highly resembles the findings observed in humans with Crouzon syndrome.

These data, together with the original description of the *Fgfr2^{C342Y}* mouse, confirm its anatomic, and not merely genetic, validity as a model for Crouzon syndrome, which can now be used to search for fundamental explanations of complex clinical problems. Accordingly, we have undertaken studies to further investigate the molecular mechanisms underlying the anomalies seen in the Crouzon mouse model. These include studies on the midface and palate, trachea, endocranial base, and cranial sutures, including surgical interventions. We have also initiated an analysis of craniofacial growth by using sequential 3D CT scan data from E17.5 mouse embryos through adult stages. Our ability to investigate these developmental processes in embryonic and fetal stages in the *Fgfr2^{C342Y}* mouse highlights its importance in understanding the etiology of Crouzon syndrome. In addition, the detailed analysis provided here will be of value as therapeutic strategies for Crouzon syndrome (such as adjuvant pharmacologic treatment) begin to emerge, because the effectiveness of these treatments on craniofacial growth can now be compared and assessed by quantitative outcome studies.

Acknowledgments. We thank Prof. Andrew Wilkie, University of Oxford, and Prof. David Ornitz, Washington University in St. Louis, for their insight and helpful comments regarding this work and our ongoing studies. We also acknowledge the efforts of Dr. V.P. Eswarakumar and the late Dr. Peter Lonai for their work in the initial generation of the mouse model.

REFERENCES

- Abe S, Wantabe H, Hirayama A, Shibuya E, Hashimoto M, Ide Y. Morphological study of the femur in osteopetrotic (op/op) mice using microcomputed tomography. *Br J Radiol.* 2000;73:1078–1082.
- Burdi AR, Kusnetz AB, Venes JL, Gebarsky SS. The natural history and pathogenesis of the cranial coronal ring articulations: implications in understanding the pathogenesis of the Crouzon craniostenotic defects. *Cleft Palate J.* 1986;23:28–39.
- Carinci F, Avantaggiato A, Curioni C. Crouzon syndrome: cephalometric analysis and evaluation of pathogenesis. *Cleft Palate Craniofac J.* 1994;31:201–209.
- Cohen MM Jr. Crouzon syndrome. In: Cohen MM Jr, MacLean RE, eds. *Craniosynostosis. Diagnosis, Evaluation, and Management.* 2nd ed. New York: Oxford University Press; 2000:361–365.
- Cohen MM Jr. Fgfs/FGFRs and associated disorders. In: Epstein CJ, Erickson RP, Wynshaw-Boris A, eds. *Inborn Errors of Development: The Molecular Basis of Clinical Disorders of Morphogenesis.* New York: Oxford University Press; 2003:380–400.
- Cohen MM Jr, Kreiborg S. Upper and lower airway compromise in the Apert syndrome. *Am J Med Genet.* 1992;44:90–93.
- Crouzon O. Dysostose cranio-faciale héréditaire. *Bull Soc Med Paris.* 1912;33:545–555.
- DeLeon VB, Zumpano MP, Richtsmeier JT. The effect of neurocranial surgery on basicranial morphology in isolated sagittal craniosynostosis. *Cleft Palate Craniofac J.* 2001;38:134–146.
- Devine P, Bhan I, Feingold M, Leonidas JC, Wolpert SM. Completely cartilaginous trachea in a child with Crouzon syndrome. *Am J Dis Child.* 1984;138:40–43.
- Don N, Sigger DC. Cor pulmonale in Crouzon's disease. *Arch Dis Child.* 1971;46:394–397.
- Eswarakumar VP, Horowitz MC, Locklin R, Morriss-Kay GM, Lonai P. A gain-of-function mutation of *Fgfr2c* demonstrates the roles of this receptor variant in osteogenesis. *Proc Natl Acad Sci U S A.* 2004;101:12555–12560.
- Ford-Hutchinson AF, Cooper DM, Hallgrímsson B, Jirik FR. Imaging skeletal pathology in mutant mice by microcomputed tomography. *J Rheumatol.* 2003;30:2659–2665.
- Gower JC. Some distance properties of latent root and vector methods used in multivariate analysis. *Biometrika.* 1966;53:325–338.
- Hartsfield JK Jr, Holmes LB. Comparison of two methods for linear measurement of ossified tissue in cleared mouse fetuses. *J Craniofac Genet Devel Biol.* 1998;8:345–350.
- Krause AC, Buchanan DN. Dysostosis craniofacialis (Crouzon). *Am J Ophthalmol.* 1939;22:140–144.
- Kreiborg S. Crouzon syndrome. A clinical and roentgencephalometric study. *Scand J Plast Reconstr Surg Suppl.* 1981a;15(suppl 18):1–198.
- Kreiborg S. Craniofacial growth in plagiocephaly and Crouzon syndrome. *Scand J Plast Reconstr Surg.* 1981b;15:187–197.
- Kreiborg S. Postnatal growth and development of the craniofacial complex in premature craniosynostosis. In: Cohen MM Jr, MacLean RE, eds. *Craniosynostosis. Diagnosis, Evaluation, and Management.* 2nd ed. New York: Oxford University Press; 2000:158–174.
- Kreiborg S, Björk A. Description of a dry skull with Crouzon syndrome. *Scand J Plast Reconstr Surg.* 1982;16:245–253.
- Kreiborg S, Marsh JL, Cohen MM Jr, Liversage M, Pedersen H, Skovby F, Børgesen SE, Vannier MW. Comparative three-dimensional analysis of CT-scans of the calvaria and cranial base in Apert and Crouzon syndromes. *J Craniomaxillofac Surg.* 1993;21:181–188.
- Lele S, Richtsmeier JT. Euclidean distance matrix analysis: a coordinate-free approach for comparing biological shapes using landmark data. *Am J Phys Anthropol.* 1991;86:415–427.
- Lele S, Richtsmeier JT. Euclidean Distance Matrix Analysis—confidence intervals for form and growth comparison. *Am J Phys Anthropol.* 1995;98:73–86.
- Lele S, Richtsmeier JT. *An Invariant Approach to the Statistical Analysis of Shapes.* Boca Raton: Chapman & Hall/CRC; 2001.
- Lozanoff S. Accuracy and precision of computerized models of the anterior cranial base in young mice. *Anat Rec.* 1992;234:618–624.
- Okajima K, Robinson LK, Hart MA, Abuelo DN, Cowan LS, Hasegawa T, Maumenee IH, Jabs EW. Ocular anterior chamber dysgenesis in craniosynostosis syndrome with a fibroblast growth factor receptor mutation. *Am J Med Genet.* 1999;85:160–170.
- Perlyn CA, Kane AA, Marsh JL, Koppel P, Clark KW, Vannier MW, Christensen GE, Knapp R, Lo LJ, Govier D. The craniofacial anomalies archive at St. Louis Children's Hospital: 20 years of craniofacial imaging experience. *Plast Reconstr Surg.* 2001;108:1862–1870.
- Qvist J, Hove HD, Welling KLK, Kreiborg S. Severe obstructive sleep apnea in a child with craniofacial anomaly. *Ugeskr Laeger.* 2004;166:2910–2912.
- Reardon W, Winter RM, Rutland P, Pulleyn LJ, Jones BM, Malcolm S. Mutations in the fibroblast growth factor receptor 2 gene cause Crouzon syndrome. *Nat Genet.* 1994;8:98–103.
- Recinos RF, Hanger C, Schaefer RB, Dawson CA, Gosain AK. Microfocal CT: a method for evaluating murine cranial sutures in situ. *J Surg Res.* 2004;116:322–329.
- Richtsmeier JT, Baxter LL, Reeves RH. Parallels of craniofacial maldevelopment in Down syndrome and Ts65Dn mice. *Dev Dyn.* 2000;217:137–145.
- Richtsmeier JT, Cole T, Valeri CJ, Krovitiz G, Lele S. Pre-operative morphology and development in sagittal synostosis. *J Craniofac Genet Dev Biol.* 1998;18:64–78.
- Wilkes D, Rutland P, Pulleyn LJ, Reardon W, Moss C, Ellis JP, Winter RM, Malcolm S. A recurrent mutation, ala391glu, in the transmembrane region of FGFR3 causes Crouzon syndrome and acanthosis nigricans. *J Med Genet.* 1996;33:744–748.
- Wilkie AOM. Craniosynostosis: genes and mechanisms. *Hum Mol Genet.* 1997;6:1647–1656.